MOLECULAR BIOLOGY

Structure of the mammalian ribosome as it decodes the selenocysteine UGA codon

Tarek Hilal[1]*†, Benjamin Y. Killam[2], Milica Grozdanović[2]‡, Malgorzata Dobosz-Bartoszek[2]§, Justus Loerke[1], Jörg Bürger[1,3], Thorsten Mielke[3], Paul R. Copeland[4], Miljan Simonović[2]*¶, Christian M. T. Spahn[1]*

The elongation of eukaryotic selenoproteins relies on a poorly understood process of interpreting in-frame UGA stop codons as selenocysteine (Sec). We used cryo-electron microscopy to visualize Sec UGA recoding in mammals. A complex between the noncoding Sec-insertion sequence (SECIS), SECIS-binding protein 2 (SBP2), and 40S ribosomal subunit enables Sec-specific elongation factor eEFSec to deliver Sec. eEFSec and SBP2 do not interact directly but rather deploy their carboxyl-terminal domains to engage with the opposite ends of the SECIS. By using its Lys-rich and carboxyl-terminal segments, the ribosomal protein eS31 simultaneously interacts with Sec-specific transfer RNA (tRNA^Sec) and SBP2, which further stabilizes the assembly. eEFSec is indiscriminate toward L-serine and facilitates its misincorporation at Sec UGA codons. Our results support a fundamentally distinct mechanism of Sec UGA recoding in eukaryotes from that in bacteria.

Translating ribosomes pause at stop codons—UAA, UAG, and UGA—which allows a protein release factor (RF) to bind and terminate protein synthesis. In a subset of mRNAs from most organisms across all domains of life, in-frame UGA codons recruit selenocysteinyl-tRNA (Sec-tRNA^Sec) to facilitate the stop-to-Sec recoding. The recoding leads to the synthesis of selenoproteins, which are required for a myriad of functions, notably the maintenance of redox and thyroid hormone homeostasis and protection of the cell membrane and DNA from oxidative damage (1). An embryonically lethal phenotype of the mouse mutant in which tRNA^Sec was deleted (2) and systematic analyses of genetic rodent models of selenoprotein deficiency (3, 4) demonstrate that selenoproteins are essential for vertebrate survival. Selenoprotein deficiency and mutations in selenoproteins cause systemic, often lethal diseases in humans (5). Despite the biological importance, the mechanism of Sec UGA recoding in eukaryotes is not well understood.

Stop-to-Sec recoding relies on a Sec-insertion sequence (SECIS) in the selenoprotein mRNA and a Sec-specific elongation factor—SelB in prokaryotes and eEFSec in eukaryotes. Although the bacterial SECIS follows Sec UGA within the open reading frame, the phylogenetically unrelated eukaryotic SECIS is in the 3′-untranslated region (3′-UTR). Prokaryotic SelB facilitates recoding on its own, but eEFSec requires a eukaryote-specific protein factor, SECIS-binding protein 2 (SBP2). Despite some conservation, the prokaryotic mechanism (6) cannot be extrapolated to eukaryotes (7). This raises questions about the architecture of the eukaryotic UGA recoding assembly (the "selenosome"), the role of SECIS and SBP2, and the molecular choreography that governs discrete steps of the process. To address these questions, we reconstituted human eEFSec, SBP2, and Ser-tRNA^Sec on mammalian 80S ribosomes that were programmed with an mRNA containing an authentic SECIS element. Using cryo–electron microscopy (cryo-EM), we visualized the early steps of Sec UGA recoding in higher eukaryotes, providing a structural basis for the distinct mechanism of selenoprotein elongation.

To produce a stable complex and position the UGA codon in the ribosomal decoding center (DC), we used a chimeric mRNA construct that harbored a cricket paralysis virus (CrPV) internal ribosome entry site (IRES) on its 5′ end (8). Sec UGA, the first coding triplet, is followed by ~900 nucleotides (nt) of firefly luciferase coding region and the 3′-UTR of rat glutathione peroxidase 4 (Gpx4) that contains the SECIS. We combined the chimeric mRNA, purified rabbit ribosomal subunits, and the functional C-terminal half of human SBP2 (residues 409–854), which is composed of a Sec-insertion domain (SID) and an RNA-binding domain (RBD) (Fig. 1A). Concurrently, we assembled a ternary complex of the guanosine triphosphatase (GTPase)–defective His^96→Ala mutant of eEFSec (eEFSec-H96A), Ser-tRNA^Sec, and guanosine 5′-triphosphate (GTP). We chose eEFSec-H96A to avoid complex disassembly from GTP hydrolysis and Ser-tRNA^Sec because of its similarity with Sec-tRNA^Sec. In the end, programmed ribosomes and ternary complex were assembled into the recoding complex immediately before vitrification (Fig. 1A).

From 13,921 selected micrographs, a total of 1,685,923 particle images were extracted and analyzed by means of multiparticle refinement (figs. S1 to S3 and table S1). A subpopulation of 77,142 particle images that corresponded to the intact selenosome yielded a reconstruction of 2.8 Å resolution (Fig. 1 and figs. S1 and S2). All recoding factors form an extended network of interactions (Fig. 1, B to E). The density for SECIS, a member of the kink-turn family of RNA structural motifs, is well resolved and is adjacent to the beak domain of the 40S. Near the SECIS core, densities for a segment of the SID and the entire RBD of SBP2 are readily visible (Figs. 1E and 2A). The opposite end of the SECIS contacts the C-terminal domain 4 (D4) of eEFSec, whereas D1, D2, and D3 reside at the GTPase-associated center (GAC). The acceptor and variable arms of Ser-tRNA^Sec are bound to eEFSec (Fig. 2A), and the anticodon loop is properly positioned in the A site of the DC, which suggests that we captured the preaccommodated state of the selenosome with the tRNA^Sec in the A/T conformation (fig. S4). The long mRNA segment that connects UGA and the SECIS is partially disordered and could not be modeled. The CrPV IRES is in the translocated state (8), which points away from the DC and rests against ES30L of the L1 stalk in the 60S (Fig. 1, C and D). We did not observe any interactions between the CrPV IRES and eEFSec, SBP2, Ser-tRNA^Sec, or the SECIS element. The absence of such interactions and the general similarity of our visualized recoding complex to canonical mammalian decoding complexes (9, 10) suggest its physiological relevance.

Our reconstruction revealed the structure of the eEFSec•GTP•Ser-tRNA^Sec complex (Figs. 1E and 2A). eEFSec-H96A resembles crystal structures of wild-type (WT) eEFSec (11) and archaeal SelB (12) (fig. S5A). When compared with the bacterial SelB, the structural conservation is preserved in D1, D2, and D3 but absent in D4 (fig. S5B). GTP is bound to the GTPase pocket in D1, but the side chains of switch 2 are disordered, which confirms the catalytically incompetent conformation of eEFSec-H96A (fig. S6A). D1 and D2 are sandwiched between H95 and uL14 of the 60S and h5 and h14 of the 40S (Fig. 2B), whereas D4 is wedged between the apical loop of SECIS and h33 of the 40S (Fig. 2D). The CCA end of tRNA^Sec positions the Ser group into the proposed Sec-binding pocket. Highly conserved

[1]Institut für Medizinische Physik und Biophysik, Charité-Universitätsmedizin Berlin, 10117 Berlin, Germany. [2]Department of Biochemistry and Molecular Genetics, University of Illinois at Chicago, Chicago, IL 60607, USA. [3]Max-Planck Institut für Molekulare Genetik, 14195 Berlin, Germany. [4]Department of Biochemistry and Molecular Biology, Rutgers-Robert Wood Johnson Medical School, Piscataway, NJ 08854, USA.
*Corresponding author. Email: tarek.hilal@fu-berlin.de (T.H.); miljan.simonovic@nih.gov (M.S); christian.spahn@charite.de (C.M.T.S)
†Present address: Research Center of Electron Microscopy and Core Facility BioSupraMol, Institute of Chemistry and Biochemistry, Freie Universität Berlin, Berlin, Germany. ‡Present address: Vaccines Analytical Development, Merck & Co., Inc., West Point, PA 19486, USA. §Present address: Cytiva, Marlborough, MA 01752, USA. ¶Present address: National Institute of General Medical Sciences, National Institutes of Health, Bethesda, MD 20892, USA.
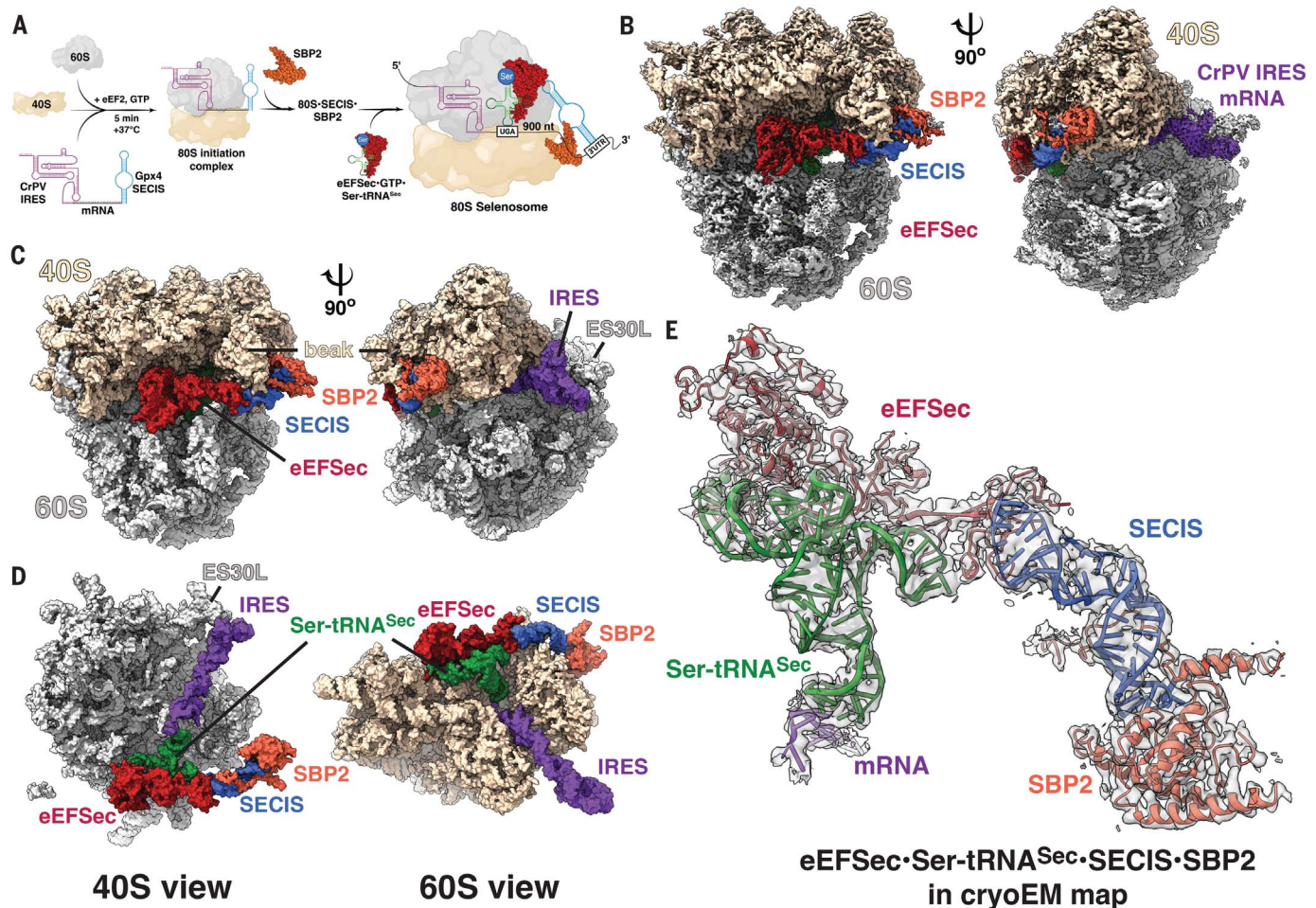
Fig. 1. The mammalian Sec UGA recoding assembly. (**A**) Reconstitution of complexes used in this study. (**B**) Three dimensional (3D) reconstruction of the assembly shown in two views related by ~90° clockwise rotation around the vertical axis. (**C**) The same views of the final model shown as a surface diagram. (**D**) The recoding complex as seen from the vantage points of the 40S (left) and 60S (right) subunits. (**E**) 3D map covering the eEFSec•GTP•Ser-tRNA^{Sec}•SECIS•SBP2 complex (cartoon). 60S is gray, 40S is sand, eEFSec•GTP is dark red, Ser-tRNA^{Sec} is dark green, SECIS is blue, SBP2 is dark orange, and the mRNA harboring CrPV IRES is purple.

Ser^{269}, Gln^{271}, and His^{274} surround Ala^{76} (fig. S7), and H-bonds with Gln^{237} lock its nucleobase in place (Fig. 2C). Phe^{273} and Arg^{285} cap the Sec-binding pocket, with Arg^{285} stabilizing the pocket through interactions with Thr^{242}. This explains the loss of function in Arg^{285}→Ala (R285A) and Arg^{285}→Asn (R285N) mutants (*11*). The hydroxyl of Thr^{242} is ~3.7 Å from the hydroxyl of Ser on Ser-tRNA^{Sec} (Fig. 2C), which suggests its importance for amino-acid selection. When accounting for the longer C-Se bond, the Se atom of Sec would be at the optimal distance of ~2.6 to 3.2 Å from Thr^{242}. Last, the eukaryote-specific loop β24–β25 (residues 522–524) in D4 of eEFSec forms an interface with the backbone of the AAR motif of SECIS (residues 1128–1130) and h33 (residues 1305–1308) of the 40S subunit (Fig. 2, D and E). Using a well-established Sec UGA readthrough reporter assay (Fig. 2F) (*13*), we

show that eEFSec promotes recoding in an SBP2- and SECIS-dependent manner in the presence of Ser-tRNA^{Sec} but not Ser-tRNA^{Ser} (Fig. 2G). Also, replacing Thr^{242} with either Val (T242V) or Leu (T242L) and Phe^{522} and Gln^{524} with Gly (F522G and Q524G) causes impairment of the readthrough activity (Fig. 2H). Taken together, our results argue that Thr^{242} is a key selectivity residue in human eEFSec. Also, just as Cys is misincorporated at Sec UGA in TXNRD1 under low Se levels (*14*), the same may occur with Ser. However, it remains to be seen whether Ser misinsertion occurs in vivo and whether selenoenzyme activity is affected.

Human eEFSec uses all its domains to engage the tRNA^{Sec} (fig. S6, center). D1, D2, and D3 bind to the acceptor-TΨC arm (fig. S6, B and C), whereas the D3–D4 linker and D4 contact the variable stem and loop (fig. S6,

D and E). The side chain of Glu^{299} establishes the tRNA^{Sec} identity through H-bonds with the Watson-Crick face of the Gly^{73} recognition base (fig. S6B). Arg^{432} and Asp^{434} from loop β19–β20 of D3 contact the minor groove of the TΨC arm (fig. S6C). The D3–D4 linker runs parallel to the variable arm where Lys^{471} interacts with a nonbridging oxygen between G47a and U47b (fig. S6D), and the variable loop is lodged against loop β22–α12 (residues 495–499) of D4 (fig. S6E). These interactions explain why mutations in and deletion of D4 had detrimental effects on eEFSec activity and selenoprotein synthesis (*15*). Although they share a conserved biological role, the eukaryotic selenosome is distinct from the bacterial one (fig. S8A), which suggests divergent UGA recoding mechanisms. In particular, the C-terminal D4 of eEFSec interacts with the variable arm of tRNA^{Sec} and
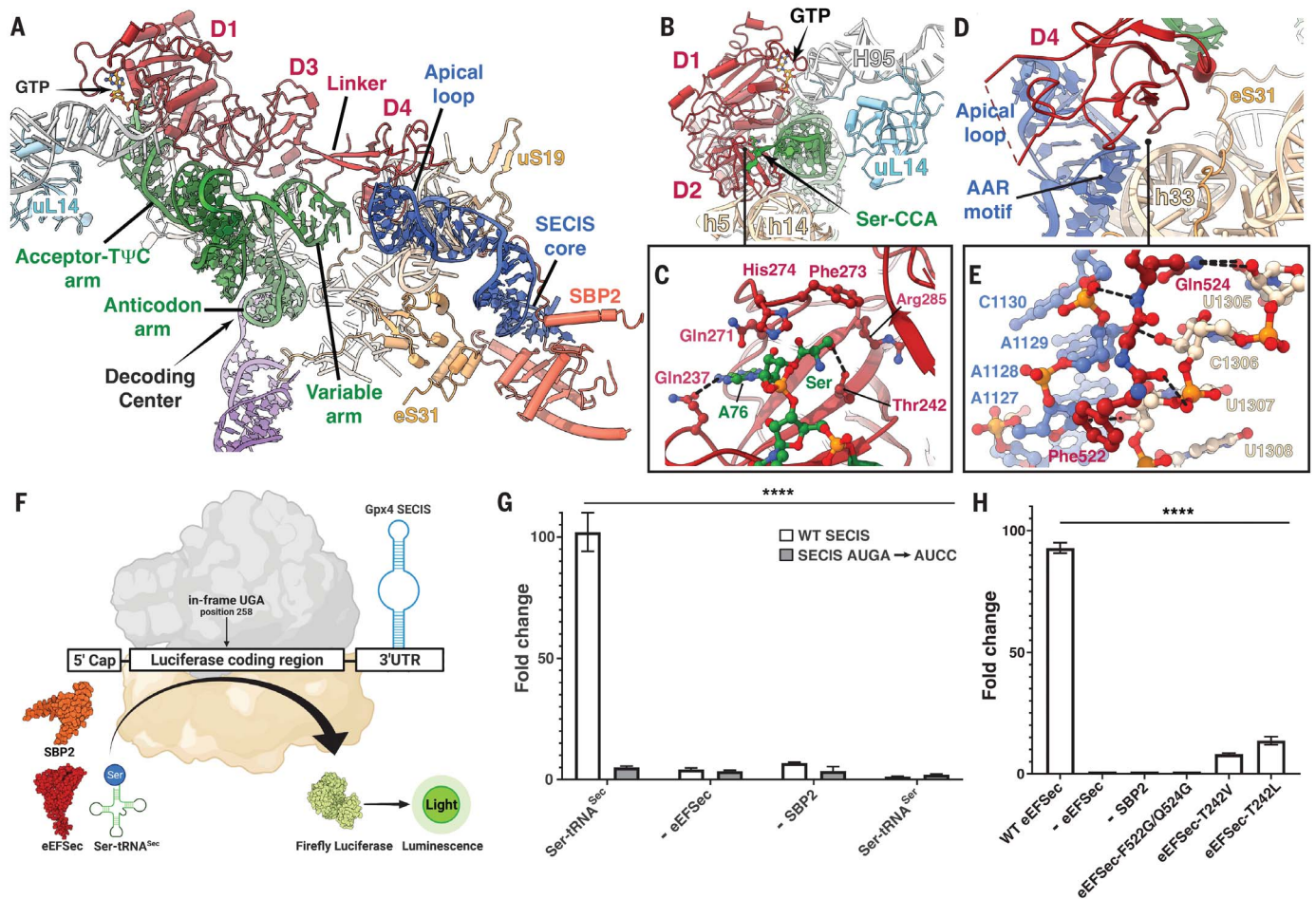
Fig. 2. Human eEFSec·GTP·Ser-tRNA^Sec on the 80S ribosome. (**A**) Side view of the eEFSec complex (cartoon) as bound to the 80S. (**B**) D1 and D2 of eEFSec rest against H95 of the 60S and h5 and h14 of the 40S. The Ser-CCA is bound to the Sec-binding pocket. The view is rotated 90° counterclockwise around the vertical axis relative to (A). (**C**) Close-up view of the Sec-binding pocket with Ser, Ala[76], and residues of the Sec-binding site shown as stick-and-ball. Dashed lines indicate H-bonds. (**D**) D4 of eEFSec is between the AAR motif of SECIS and h33 of the 40S. The view is rotated 90° clockwise around the vertical axis relative to (A). (**E**) Close-up view of the interface between AAR motif, h33, and D4. (**F**) The Sec UGA readthrough assay based on the luciferase reporter. (**G**) Ser-tRNA^Sec, but not Ser-tRNA^Ser, supports the SBP2-SECIS–dependent Sec UGA readthrough. Activity levels are presented as fold change over the control sample. White and gray bars correspond to WT and AUCC mutant SECIS, respectively. (**H**) T242L, T242V, and F522G/Q524G mutants lost the readthrough activity.

points away from the mRNA channel (fig. S8, A and B), whereas the bacterial D4 is rotated ~90° around the linker, does not interact with the variable arm, and binds near the mRNA entry channel (fig. S8C) (6).

The mammalian SECIS, which is derived from the 3′-UTR of Gpx4 (Fig. 3A), adopts a Form II structure that is characterized by two nearly coaxial stems that connect the GA quartet and AUGA bulge on one end and two loops and the essential AAR motif on the opposite, apical end (Fig. 2G). The basal stem, or helix I, is disordered in our map. The AUGA bulge, or the SECIS core, folds into a kink-turn motif, which serves as the SBP2-binding site (Fig. 3, A and B). Sitting atop Leu[707], U1112 forms H-bonds with the invariant Arg[731] of SBP2, which suggests its relevance for complex formation (Fig. 3C). The rest of the bulge is

structurally important, as illustrated by the inability of the AUGA→AUCC mutant to support recoding (Fig. 2G). On the opposite end are the apical stem, the apical loop, and the AAR motif, which is characterized by three unpaired adenosines (Fig. 3A). Replacing unpaired AAA with AUG hinders recoding (16), but the absence of sequence-specific interactions with the AAR motif may rationalize why some SECIS elements carry the CCR motif instead (17). Nonetheless, our structure uncovered insights about SECIS, a noncoding RNA element that regulates selenoprotein synthesis in higher organisms.

We modeled the N-terminal segment of the SID (residues 429–475) and RBD (residues 625–780) of SBP2 (Fig. 3B). Residues 429–437 fold into a fishhook-like structure that anchors against h33 of the 18S ribosomal RNA (rRNA).

The subsequent segment (residues 441–446) forms a parallel β-strand that leans against the C terminus of eS31, which effectively expands the β sheet of the zinc-finger motif of this ribosomal protein (Fig. 3B). With its Lys-rich motif, eS31 reaches the anticodon arm of tRNA^Sec (fig. S9), but the 84 N-terminal residues are disordered, which allows expansion of the A site and accommodation of an enlarged tRNA^Sec variable arm. Residues 448–455 of the SID run along the major groove of SECIS (Fig. 3B) without establishing sequence-specific contacts. The SID in our structure ends with an α helix (residues 456–475), which is almost perpendicular to helix II of SECIS and is near the β1–α3 loop ([701]IQSKG[705]) of the RBD (Fig. 3B). The ribosomal protein uS19 binds to the opposite side of helix II, which further stabilizes the complex (Fig. 3B). Using
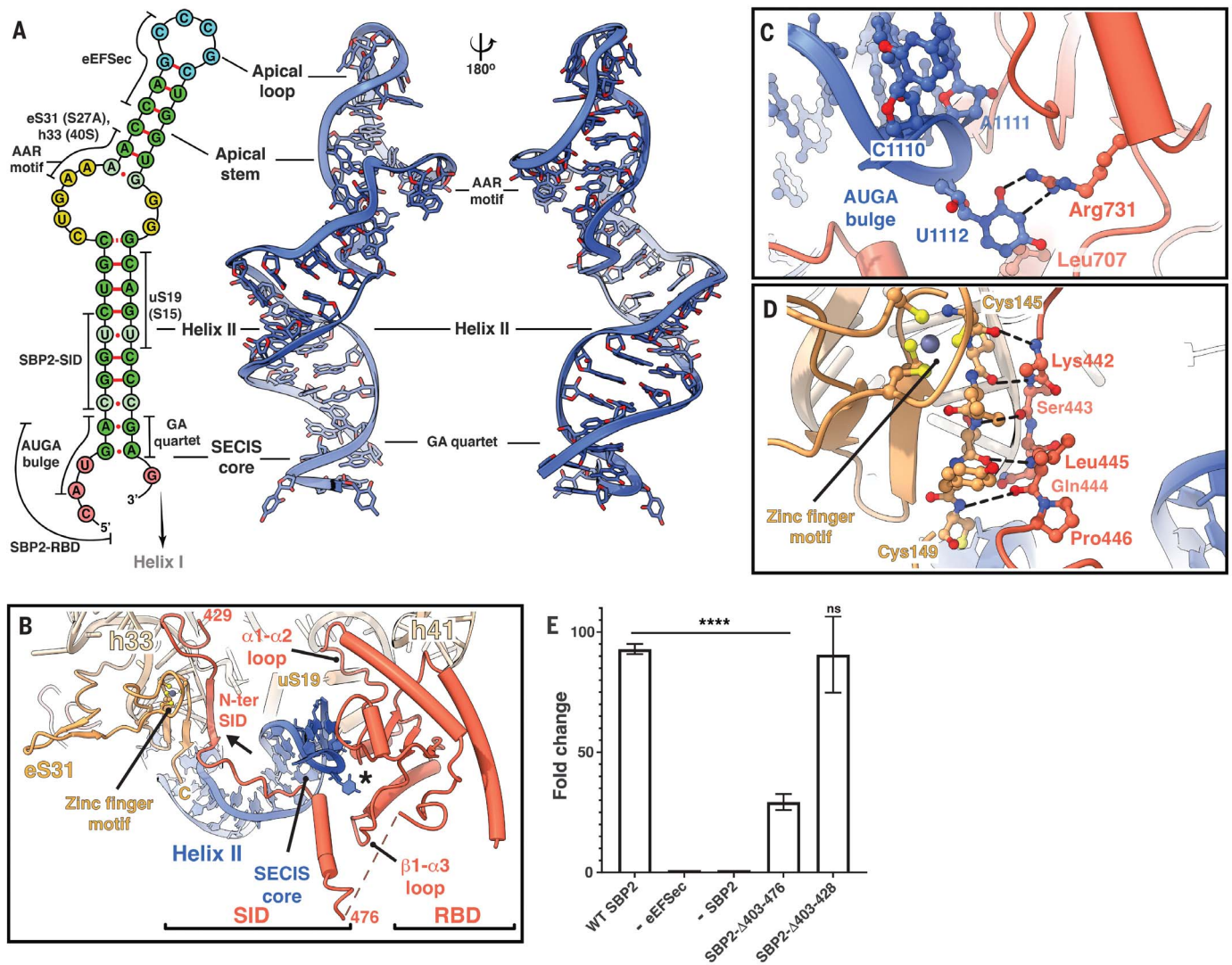
Fig. 3. Human SBP2•SECIS captured on the translating ribosome. (**A**) Secondary structure diagram (left) and two views of the 3D structure of the Form II Gpx4 SECIS (right). Major interactions are marked; base pairs are green; and loops are pink, yellow, and light blue. Solid red lines indicate Watson-Crick base pairs, dashed lines are non–Watson-Crick pairs, and red dots are wobble pairs. Color coding is the same as in Fig. 1. (**B**) RBD binds to the SECIS core (asterisk). The SID interacts with the zinc finger of eS31 (arrow). Contacts between helix II of the SECIS and uS19 and eS31 stabilize the complex. (**C**) Close-up view of interactions between Arg[731] of RBD and U1112 of SECIS. (**D**) N-terminal segment of SID (residues 442–446) forms a parallel β-strand to the C terminus of eS31. (**E**) Only deletion of residues 403–476 from SBP2 (Δ403-476) abolishes Sec UGA readthrough activity.

luciferase reporter assay (Fig. 2F), we show that SBP2 that lacks residues 403–428 (SBP2-Δ428), but not 403–476 (SBP2-Δ476), supports Sec UGA readthrough (Fig. 3E). This suggests that residues 429–476 of the SID are important for binding of SBP2 to the ribosome and explains why mutations in the same region of rat SBP2 substantially diminished Sec incorporation efficiency (18, 19). Furthermore, RBD of SBP2 adopts an L7Ae protein fold and binds to the conserved kink-turn motif of the SECIS. The RBD is locked in place through interactions of conserved [654]RFQDR[658], [663]DPVKA[667], and [680]VLKHLKL[686] motifs (fig. S10) with ribosomal protein uS19 and h41 of the 40*S* (Fig. 3B). This illuminates why mutations

in these motifs hindered ribosome binding and Sec incorporation activity, but not SECIS binding (19). Last, we rationalize effects of the disease-associated missense mutations Glu[679]→Asp (E679D) and Cys[691]→Arg (C691R) (fig. S11A) (20, 21). Although the effects of E679D are neutral, C691R probably compromises SBP2 structure because of steric clashes of Arg[691] with Ile[693], Pro[724], Val[726], Ile[749], Phe[759], and Met[762] (fig. S11, B and C).

We investigated whether binding to the 80*S* of SBP2•SECIS alone could poise the ribosome for Sec UGA recoding. To this end, we determined the structure of the 80*S*•SBP2•SECIS complex at 3.1 Å resolution (Fig. 4A and fig. S3). We found that SBP2 and SECIS are bound to

the beak of the 40*S* in the same manner as in the preaccommodated state structure of the complete selenosome (Fig. 4A). The mRNA follows a similar trajectory, which suggests that its conformation is independent from the eEFSec ternary complex binding and the recoding step itself. We thus conclude that the SBP2• SECIS binding to 80*S* is a prerequisite for the eEFSec•GTP•Sec-tRNA[Sec] ternary complex anchoring, which is consistent with the observation that the eukaryotic SECIS promotes Sec incorporation in cis when placed >55 nt downstream of the Sec codon (22). Last, SBP2•SECIS is not found in a position to prevent translation termination, which explains why RFs terminate selenoprotein
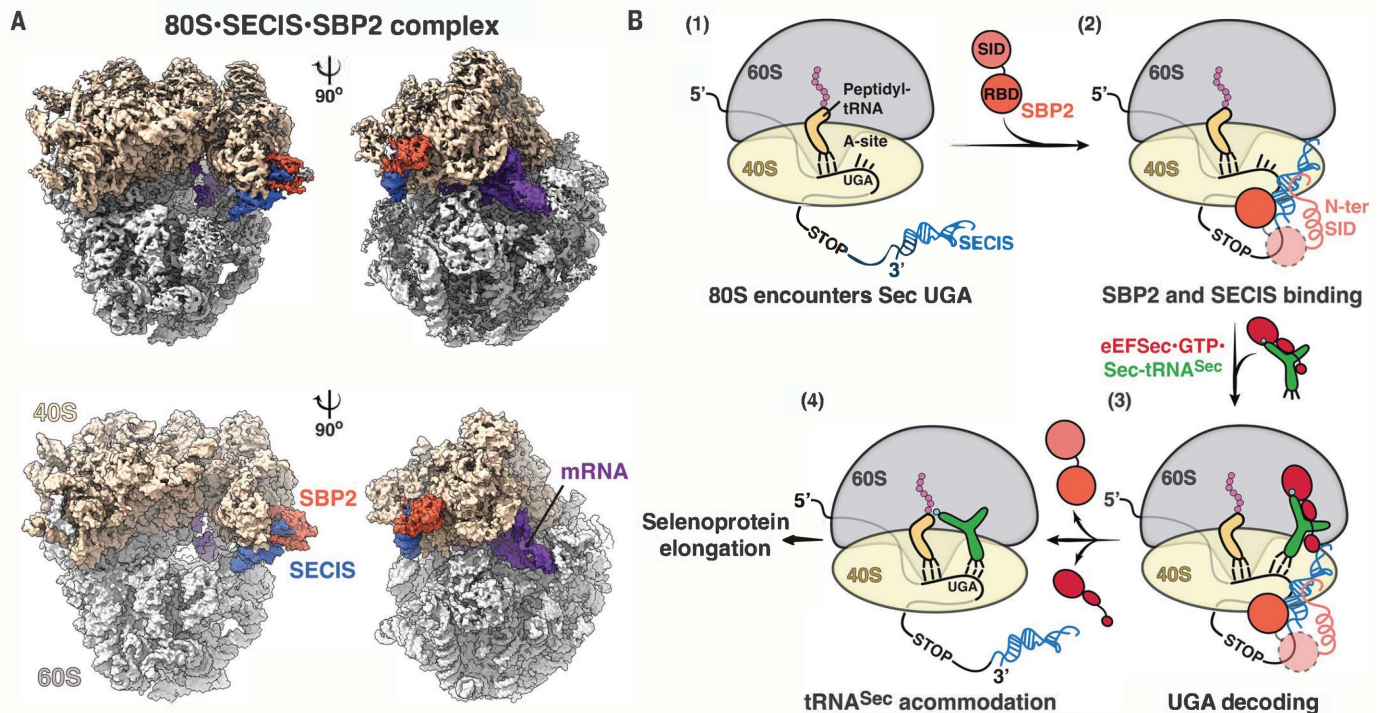
Fig. 4. Eukaryotic selenoprotein elongation at Sec UGA codons. (**A**) Cryo-EM map (top) and surface diagram (bottom) of 80S•SECIS•SBP2. (**B**) Proposed mechanism of Sec UGA recoding in eukaryotes. (1) 80S stalls at an in-frame UGA codon. (2) The RBD binds to the apical loop of SECIS, the mRNA folds over, SBP2•SECIS binds to the 40S, and the N terminus of the SID contacts eS31. This step could occur before ribosome stalling. (3) eEFSec•GTP delivers Sec-tRNA^{Sec} to the 80S and adopts a preaccommodated state conformation. (4) After GTP hydrolysis, eEFSec dissociates from the assembly, Sec-tRNA^{Sec} accommodates, and peptide bond synthesis and selenoprotein elongation occur. Steps 2 and 3 are visualized in this work.

synthesis at UGA codons when Sec insertion fails (*23, 24*).

Although we cannot rule out that IRES and Ser-tRNA^{Sec} may have imposed kinetic and conformational constraints on programmed ribosomes, our structures allowed visualization of the long-sought early steps of selenoprotein elongation at Sec UGA codons in eukaryotes, leading to a revised model of the process (Fig. 4B). During translation of selenoprotein mRNAs, the SBP2•SECIS complex binds to the head domain of the 40S subunit. The RBD of SBP2 binds to the SECIS base, whereas the N-terminal part of the SID latches onto the 40S through contacts with the rRNA and eS31. The prebound SBP2•SECIS forms a docking site on the stalled ribosome for eEFSec•GTP•Sec-tRNA^{Sec} (Fig. 4B). The EF-Tu–like domain of eEFSec binds to the GAC, and D4 binds to the apical loop of the SECIS, opposite from the RBD. eEFSec clasps the A/T conformation of Sec-tRNA^{Sec} with the variable arm contacting the Lys-rich domain of eS31, which completes the preaccommodated state of the selenosome. Subsequent events remain unclear, which warrants detailed structural analyses. After adopting the GTPase activated state, the CCA end of Sec-tRNA^{Sec} is liberated from eEFSec. eEFSec

dissociates from the ribosome, which leads to the departure of SECIS and SBP2. Sec-tRNA^{Sec} accommodates, and the peptide bond forms between an incoming Sec and the P-site peptidyl-tRNA, which ultimately completes the elongation step of a nascent selenoprotein at the UGA codon.

REFERENCES AND NOTES

1. Y. Zhang et al., *Antioxidants* **9**, 383 (2020).
2. M. R. Bösl, K. Takaku, M. Oshima, S. Nishimura, M. M. Taketo, *Proc. Natl. Acad. Sci. U.S.A.* **94**, 5531–5534 (1997).
3. M. V. Kasaikina, D. L. Hatfield, V. N. Gladyshev, *Biochim. Biophys. Acta* **1823**, 1633–1642 (2012).
4. G. K. Sarangi, L. R. White, S. Castellano, *eLS* 10.1002/9780470015902.a0026518 (2017).
5. U. Schweizer, N. Fradejas-Villar, *FASEB J.* **30**, 3669–3681 (2016).
6. N. Fischer et al., *Nature* **540**, 80–85 (2016).
7. J. N. Gonzalez-Flores, S. P. Shetty, A. Dubey, P. R. Copeland, *Biomol. Concepts* **4**, 349–365 (2013).
8. M. Muhs et al., *Mol. Cell* **57**, 422–432 (2015).
9. T. V. Budkevich et al., *Cell* **158**, 121–131 (2014).
10. S. Shao et al., *Cell* **167**, 1229–1240.e15 (2016).
11. M. Dobosz-Bartoszek et al., *Nat. Commun.* **7**, 12941 (2016).
12. M. Leibundgut, C. Frick, M. Thanbichler, A. Böck, N. Ban, *EMBO J.* **24**, 11–22 (2005).
13. N. Gupta, L. W. DeMong, S. Banda, P. R. Copeland, *J. Mol. Biol.* **425**, 2415–2422 (2013).
14. X. M. Xu et al., *Proc. Natl. Acad. Sci. U.S.A.* **107**, 21430–21434 (2010).
15. J. N. Gonzalez-Flores, N. Gupta, L. W. DeMong, P. R. Copeland, *J. Biol. Chem.* **287**, 38936–38945 (2012).
16. M. J. Berry, L. Banu, J. W. Harney, P. R. Larsen, *EMBO J.* **12**, 3315–3322 (1993).
17. K. V. Korotkov, S. V. Novoselov, D. L. Hatfield, V. N. Gladyshev, *Mol. Cell. Biol.* **22**, 1402–1411 (2002).
18. J. Donovan, K. Caban, R. Ranaweera, J. N. Gonzalez-Flores, P. R. Copeland, *J. Biol. Chem.* **283**, 35129–35139 (2008).
19. K. Caban, S. A. Kinzy, P. R. Copeland, *Mol. Cell. Biol.* **27**, 6350–6360 (2007).
20. E. Schoenmakers et al., *J. Clin. Invest.* **120**, 4220–4235 (2010).
21. J. Fu et al., *J. Clin. Endocrinol. Metab.* **105**, e6–e11 (2020).
22. G. W. Martin III, J. W. Harney, M. J. Berry, *RNA* **2**, 171–182 (1996).
23. A. Mehta, C. M. Rebsch, S. A. Kinzy, J. E. Fletcher, P. R. Copeland, *J. Biol. Chem.* **279**, 37852–37859 (2004).
24. S. B. Kotini, F. Peske, M. V. Rodnina, *Nucleic Acids Res.* **43**, 6426–6438 (2015).

SUPPLEMENTARY MATERIALS

science.org/doi/10.1126/science.abg3875
Materials and Methods
Figs. S1 to S11
Table S1
References (*25–45*)
MDAR Reproducibility Checklist

View/request a protocol for this paper from *Bio-protocol*.

Science

Structure of the mammalian ribosome as it decodes the selenocysteine UGA codon

Tarek HilalBenjamin Y. KillamMilica Grozdanovi#Malgorzata Dobosz-BartoszekJustus LoerkeJörg BürgerThorsten MielkePaul R. CopelandMiljan Simonovi#Christian M. T. Spahn

How to make selenoproteins

In all domains of life, the essential trace element selenium is incorporated into selenoproteins as the amino acid selenocysteine during protein translation. Specialized protein and RNA factors assist selenocysteine transfer RNA to reinterpret specific UGA codons, not as a signal to end protein synthesis, but rather as a sign for selenocysteine insertion. Hilal *et al.* used cryo–electron microscopy to trap and visualize the mammalian ribosome as it decodes the selenocysteine UGA codon. An unforeseen extended network of interactions between key molecular players facilitates the recoding event, thereby providing a basis for further studies of this fundamental biological process. —DJ

View the article online
https://www.science.org/doi/10.1126/science.abg3875
Permissions
https://www.science.org/help/reprints-and-permissions

Use of this article is subject to the Terms of service